# Assessment of error bounds of solutions obtained from Reduced Order Methods

Vikesh Navinchandre
vikesh.navinchandre@tecnico.ulisboa.pt

Instituto Superior Técnico, Lisbon, Portugal

September 2021

**Abstract**

Associated with the continuous advances in both modeling and computing resources, numerical simulations became an everyday tool in science and engineering activities [1]. Yet, for multi-parameter models, using classical numerical techniques, where one solution is computed for each set of parameters, those approaches suffer from the so called *curse of dimensionality*, due to the exponentialy large number of solutions involved. Alternative approaches, such as reduced order methods, have been developed to avoid this problem. This work is focused on the application of one of these techniques, the Proper Generalized Decomposition (PGD) for obtaining approximated complementary solutions, one compatible and other equilibrated, for the essential unknowns of two simple problems of plane elasticity. These solutions are used to compute global and local bounds of their errors and based on this information it is possible to drive a mesh adaptivity process, which accounts for the effect of varying the parameters.

For the problems analysed, namely a square plate subjected to a traction and a plate fixed at both ends subjected to a pressure on top, even using finer meshes, it is observed that the number of modes required to obtain an accurate solution turns out to be smaller than a few dozens. However, for a given level of accuracy, using finer meshes generally implies a large number of modes, since more details of the model are being captured. It is also observed that higher values for the bounds of the error of local outputs occur in general when the materials have extreme opposite values of the Young's modulus and these bounds are smaller when the properties are equal. Finally, using a mesh adaptivity process oriented for a given quantity of interest, led in general to smaller values for the error on that local output than an uniform refinement or the refinement based on either the global error indicator or the local error indicator for another quantity. Using the global error indicator to drive the adaptivity process led to smaller global errors for the solutions and to a balance between the different local error bounds.

**Keywords:** 2D Elasticity, Model Order Reduction, Proper Generalized Decomposition, Quantities of Interest, Errors Estimation, Adaptivity Process

## 1. Introduction

### 1.1. Motivation

This work is focused on the application of the Proper Generalized Decomposition (PGD). This technique operates by constructing a separated representation for the solution of the problem involving *a priori* unknown functions of the model parameters, such that:

$$u(x_1, x_2, ..., x_n) = \sum_{i=1}^{\mathcal{N}} F_i^1(x_1) \times ... \times F_i^n(x_n)$$

where the number of terms $\mathcal{N}$ and the functions $F_i^j(x_j)$ are unknown *a priori*.

The complexity of the PGD scales linearly with the dimension of the space in which the model is defined, instead of the exponentially-growing complexity characteristic of mesh based discretization techniques [2]. Considering a model defined in a parametric space of dimension $D = 3$ and using $M = 10$ points to discretize the parametric domain, results in $\mathcal{N} \times M \times D = \mathcal{N} \times 30$ solutions to compute, instead of the $M^D = 10^3$ required for a classical mesh-based numerical technique approach.

Since the PGD, as most numerical techniques, provides an approximation of the solution, it is cru-

cial to control its errors. In this work, the dual error analysis technique is explored, which consists in computing error bounds based on two complementary solutions, one compatible and other equilibrated. This information of the errors, is then used to drive an adaptivity refinement process.

### 1.2. Objectives

This work is developed based on the work done in the PhD Thesis of Jonatha Reis, recently concluded [3], seeking to identify by means of its application to two simple 2D elasticity problems, advantages and disadvantages of this approach. To achieve this, the following objectives are estabilished:

- Formulate the problem to analyse and the approaches available to compute an approximate solution;
- Formulate the PGD separated representation of the solution as a function of the material properties;
- Formulate the dual error analysis technique and its application to adaptivity process;
- Analyse the results of PGD and mesh adaptivity process on each problem, as a way to identify its pros and cons.

## 2. Theoretical Background

### 2.1. 2D Elasticity and FEM formulations

Consider the 2D linear elastic body defined in the domain $\Omega \subset \mathbb{R}^2$ with boundary $\Gamma$, subjected to body forces $b$, tractions $\bar{t}$, and imposed displacements $\overline{u}$ on the boundary, which is decomposed in Neumann, $\Gamma_N$, and Dirichlet, $\Gamma_D$, conditions, such that $\Gamma_N \cap \Gamma_D = \emptyset$.

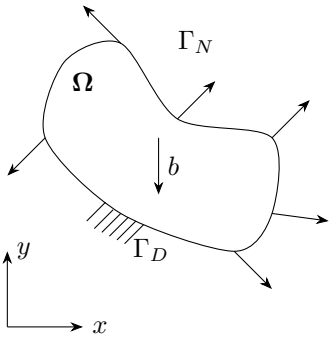


Figure 1: Representation of the reference problem.

The unknowns considered in the problem in Fig. 1, are the stresses, $\sigma$, and the displacements, $u$, represented by the vectors in expression (1).

$$\sigma = \begin{bmatrix} \sigma_{xx} \\ \sigma_{yy} \\ \sigma_{xy} \end{bmatrix} \qquad u = \begin{bmatrix} u_x \\ u_y \end{bmatrix} \tag{1}$$

In the $(x, y)$ cartesian reference system the compatibility equation is given by:

$$\varepsilon = Du \qquad D = \begin{bmatrix} \frac{\partial}{\partial x} & 0 \\ 0 & \frac{\partial}{\partial y} \\ \frac{\partial}{\partial y} & \frac{\partial}{\partial x} \end{bmatrix} \tag{2}$$

The constitutive relation is expressed by:

$$\varepsilon = \mathcal{C}\sigma \tag{3}$$

where for an isotropic material with Young's modulus $E$ and Poisson ratio $\nu$, the elasticity operator $\mathcal{C}$, for plane stress state, is given by:

$$\mathcal{C} = \frac{1}{E} \begin{bmatrix} 1 & -\nu & 0 \\ -\nu & 1 & 0 \\ 0 & 0 & 2(1+\nu) \end{bmatrix} \tag{4}$$

A compatible finite element formulation can be used to compute an approximation for the unknowns in expression (1). For this approach, as the starting point, an approximation for the displacement field $u_h$ must be given. Then the fundamental equation is expressed by:

$$\mathcal{K}\,\widehat{u} = \widehat{f} \tag{5}$$

where $\mathcal{K}$ is the global stiffness matrix, $\widehat{u}$ is the vector of nodal displacements and $\widehat{f}$ is the vector of equivalent nodal forces. Using this approach an approximation for the generalized displacement field $u_h$ is obtained which strongly satisfies compatiblity, while equilibrium is imposed in a weak form [4].

An hybrid-equilibrium formulation approach can also be applied to approximate the unknowns (1). For this approach, as the starting point, an approximation for the stress field $s_h$ and boundary displacements $v_h$ must be given. Then the resulting system is given by:

$$\begin{bmatrix} -\mathcal{F} & \mathcal{D}^T \\ \mathcal{D} & 0 \end{bmatrix} \left\{ \begin{array}{c} \widehat{s} \\ \widehat{v} \end{array} \right\} = \left\{ \begin{array}{c} \widehat{e} \\ \widehat{t} \end{array} \right\} \tag{6}$$

where $\mathcal{F}$ is the flexibility matrix, $\widehat{e}$ is the work of the imposed displacements and deformation on the auto-equilibrated stress basis and $\widehat{t}$ is the work of applied tractions on the boundary displacements basis. Using this approach, an approximation for the generalized stress field $s_h$ is obtained, that satisfies equilibrium strongly, and an approximation for the generalized boundary displacements $v_h$, which weakly satisfies compatiblity together with the associated strains [4].

### 2.2. PGD Separated Representation

The main objective is to obtain the solution of the problem as a function of the material properties.

Therefore, a vector $\mu$ with $n_p$ parameters $\mu_1, \mu_2, ..., \mu_{n_p}$ is defined, consisting of the material properties, where each is defined in its own domain $\Omega_i \subset \mathbb{R}$, with $i = 1, 2, ..., n_p$. The vector of the parameters $\mu$ is defined as $\mu \subset \Omega_\mu = \Omega_1 \times \Omega_2 \times ... \times \Omega_{n_p} \subset \mathbb{R}^{n_p}$. The finite element formulations, presented in Sec. 2.1 are used to transform the continuous problem into a discrete one, so that the PGD algebraic equation can be solved.

The PGD parametric solutions for the problem unknowns are given by:

$$\widehat{u}(\mu) \approx \widehat{u}^{n_k}_{PGD}(\mu) = \sum_{m=1}^{n_k} \overline{u}^m \prod_{i=1}^{n_p} U_i^m(\mu_i) \tag{7}$$

$$\widehat{s}(\mu) \approx \widehat{s}^{n_s}_{PGD}(\mu) = \sum_{m=1}^{n_s} \overline{s}^m \prod_{i=1}^{n_p} S_i^m(\mu_i) \tag{8}$$

where $n_k$ and $n_s$ corresponds to the number of modes used in the approximation, $\overline{u}^m$ and $\overline{s}^m$ the space functions that describes, in each mode, the displacement and the stress field, and $U_i^m(\mu_i)$ or $S_i^m(\mu_i)$ are the coefficients that defines the weight related to each parameter $\mu_i$. The application of the PGD provides, for the problem under analysis, a pair of approximated solutions, one compatible, $u_k$, and the other equilbrated, $\sigma_s$.

### 2.3. Integration of the Separated Representation

Since the solutions are represented in a separated form, the evaluation of its integrals is computationally inexpensive. As an example, consider the integral over the domain $\Omega_\mu = \Omega_{\mu_1} \times \Omega_{\mu_2}$ of a generic function $F(\mathbf{x}, \mu_1, \mu_2)$:

$$\int_{\Omega_{\mu_1} \times \Omega_{\mu_2}} F(\mathbf{x}, \mu_1, \mu_2)\, d\mu_1\, d\mu_2 \tag{9}$$

where $\mathbf{x}$ stands for the spacial coordinates and $\mu = \{\mu_1, \mu_2\}$ the vector of the material parameters. As the problem stands, the integral must be computed in $\Omega_{\mu_1} \times \Omega_{\mu_2}$ for each value of $\mathbf{x}$. But, since the solution for $F(\mathbf{x}, \mu_1, \mu_2)$ is available in a separated form, within the PGD framework the integral yields:

$$\begin{aligned} &\int_{\Omega_{\mu_1} \times \Omega_{\mu_2}} \sum_{i=1}^{\mathcal{N}} F_i^x(\mathbf{x}) \times F_i^{\mu_1}(\mu_1) \times F_i^{\mu_2}(\mu_2)\, d\mu_1\, d\mu_2 = \\ &= \sum_{i=1}^{\mathcal{N}} F_i^x(\mathbf{x}) \left( \int_{\Omega_{\mu_1}} F_i^{\mu_1}(\mu_1)\, d\mu_1 \right) \left( \int_{\Omega_{\mu_1}} F_i^{\mu_2}(\mu_2)\, d\mu_2 \right) \end{aligned} \tag{10}$$

It is possible to see that the integral over $\Omega_{\mu_1} \times \Omega_{\mu_2}$ is decoupled into one-dimensional integrals over $\Omega_{\mu_1}$ and $\Omega_{\mu_2}$. This concept can be generalized for a model defined with $n_p$ parameters, so that in the PGD framework, the integral in $\Omega_{\mu_1} \times \Omega_{\mu_2} \times ... \times \Omega_{n_p}$ is transformed into a series of one-dimensional problems for each $\Omega_i$. This is an essential characteristic of the PGD numerical technique, allowing to tackle high-dimensional models while avoiding the curse of dimensionality.

### 2.4. Error Bounds

#### 2.4.1 Global Error Bounds

Given a pair of complementary solutions, one compatible and the other equilibrated, we can relate the energy of the difference of both solutions, $\epsilon^2$, with the energy of their errors as:

$$\epsilon^2 = \int_\Omega (\sigma_k - \sigma_s)(\varepsilon_k - \varepsilon_s)\, d\Omega \geq \begin{cases} \int_\Omega (\sigma - \sigma_s)(\varepsilon - \varepsilon_s)\, d\Omega \\ \int_\Omega (\sigma - \sigma_k)(\varepsilon - \varepsilon_k)\, d\Omega \end{cases} \tag{11}$$

Which, using the elastic constitutive relations, can be expressed as:

$$\epsilon^2 = \int_\Omega (\varepsilon_k^T \mathcal{C} \varepsilon_k + \sigma_s^T \mathcal{C}^{-1} \sigma_s - 2\sigma_s^T \varepsilon_k)\, d\Omega = \sum_{e=1}^{n_e} \epsilon^2_{[e]} \tag{12}$$

Thus, the global error bound, $\epsilon^2$, is obtained as a sum of the elemental errors contribution.

#### 2.4.2 Local Outputs and Error Bounds

In the context of a project, obtaining a displacement or reaction values local outputs at specific regions of the structure is extremely important for the design and safety verification tasks. To obtain these values, a virtual problem must also be defined, with its nature (displacement or force) and also its weight function, depending on the local output to be determined.

The local output associated with the exact displacement field, $\mathcal{L}_k(u)$, can be bounded [4]:

$$\tilde{\mathcal{L}}_k(\sigma_a) - \epsilon_{a_{local}} \leq \mathcal{L}_k(u) \leq \tilde{\mathcal{L}}_k(\sigma_a) + \epsilon_{a_{local}} \tag{13}$$

With the corrected average local output, $\tilde{\mathcal{L}}_k(\sigma_a)$, and the square of the error bound, $\epsilon^2_{a_{local}}$, given by:

$$\tilde{\mathcal{L}}_k(\sigma_a) = \frac{1}{2} \int_\Omega (\overline{\sigma}_s^T\, \mathcal{C}\, \sigma_s + \overline{\sigma}_s^T\, \varepsilon_k + \overline{\varepsilon}_k^T\, \mathcal{C}^{-1}\, \varepsilon_k + \overline{\varepsilon}_k^T\, \sigma_s)\, d\Omega \tag{14}$$

$$\left( \frac{1}{2}\, \overline{\epsilon}\, \epsilon \right)^2 = \epsilon^2_{a_{local}} = \frac{1}{8} \sum_e^{n_e} (\epsilon^2\, \overline{\epsilon}^2_{[e]} + \epsilon^2_{[e]}\, \overline{\epsilon}^2) \tag{15}$$

Similar expressions are defined for reaction values $\mathcal{L}_s(\sigma)$.

### 2.5. Adaptivity Process

The equations previously presented for specific values of the parameters, are now extended to all the parametric domain.

The global error in equation (12), written as a function of the material parameters, is integrated in the space of the parameters, obtaining a global error indicator:

$$\Psi_{global} = \int_{\Omega_\mu} \epsilon^2(\mu)\, d\Omega_\mu \tag{16}$$

Similarly, using equation (15), writing it as a functions of the material parameters and integrating in the space of the parameters, results in a local error indicator:

$$\Psi_{local} = \int_{\Omega_\mu} \epsilon^2_{a_{local}}(\mu)\, d\Omega_\mu \tag{17}$$

## 3. PGD Implementation

The following scheme presents the *Matlab* program developed by Dr. Jonatha Reis, that applies the PGD numerical technique and also the mesh adaptivity refinement process, based on the two complementary PGD solutions, one compatible, the other equilibrated.

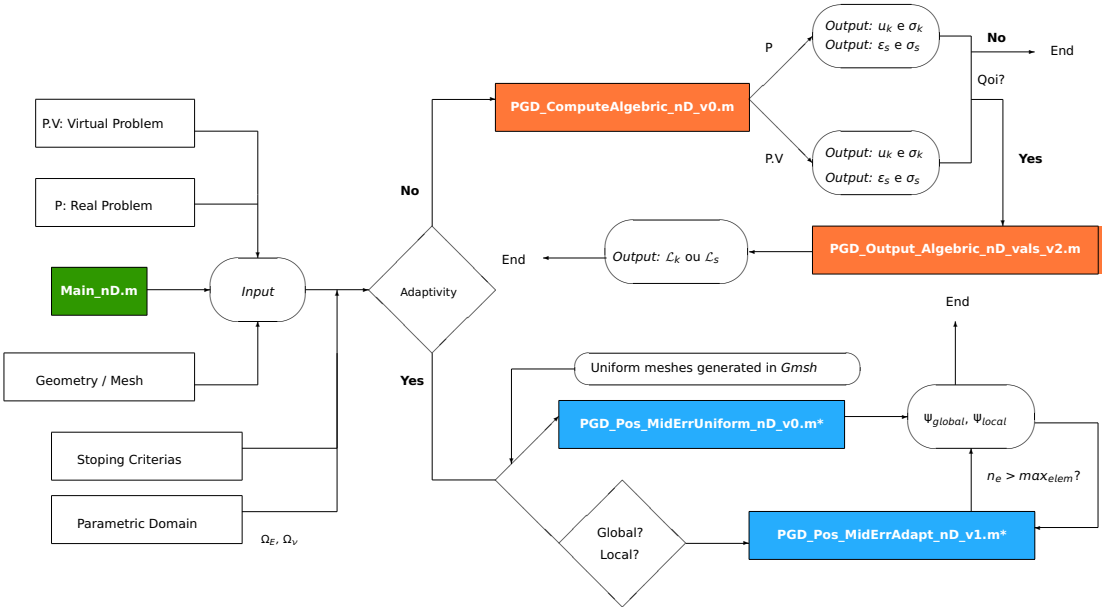


Figure 2: Scheme of the program in *Matlab* environment that implements the PGD numerical technique and mesh adaptivity process.

## 4. Results and Discussion

### 4.1. Square Plate

Consider the example shown in Fig. 3, of a square plate with two materials subjected to a traction (right) and its symmetry simplification (left), which in the homogeneous case, has an analytical solution:

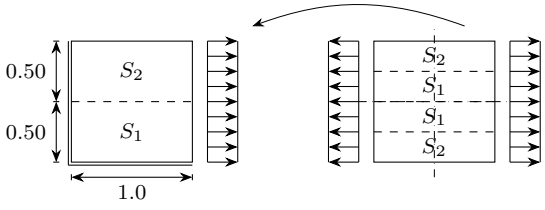


Figure 3: Square plate (right) and symmetry simplifcation (left)

$$\begin{Bmatrix} \sigma_{xx} \\ \sigma_{yy} \\ \sigma_{xy} \end{Bmatrix} = \begin{Bmatrix} 1.0 \\ 0 \\ 0 \end{Bmatrix} \qquad \begin{Bmatrix} \varepsilon_{xx} \\ \varepsilon_{yy} \\ \varepsilon_{xy} \end{Bmatrix} = \begin{Bmatrix} \frac{1}{E} \\ -\frac{\nu}{E} \\ 0 \end{Bmatrix}$$

Fig. 4 and Fig. 5, shows the PGD constuction of the solution for the equilibrated stress component $\sigma_{xx}$ and the compatible displacement field $u$, respectively, at the 4 corners of the parametric domain when the problem is solved in $\Omega_E = [0.1; 2.1]$ and $\Omega_\nu = 0.3$. In general, the number of modes to achieve an accurate solution is found to be smaller than a few dozens. It can be seen that the modes of each case are represented by the same space functions, varying just its weights depending on the parameter combination.

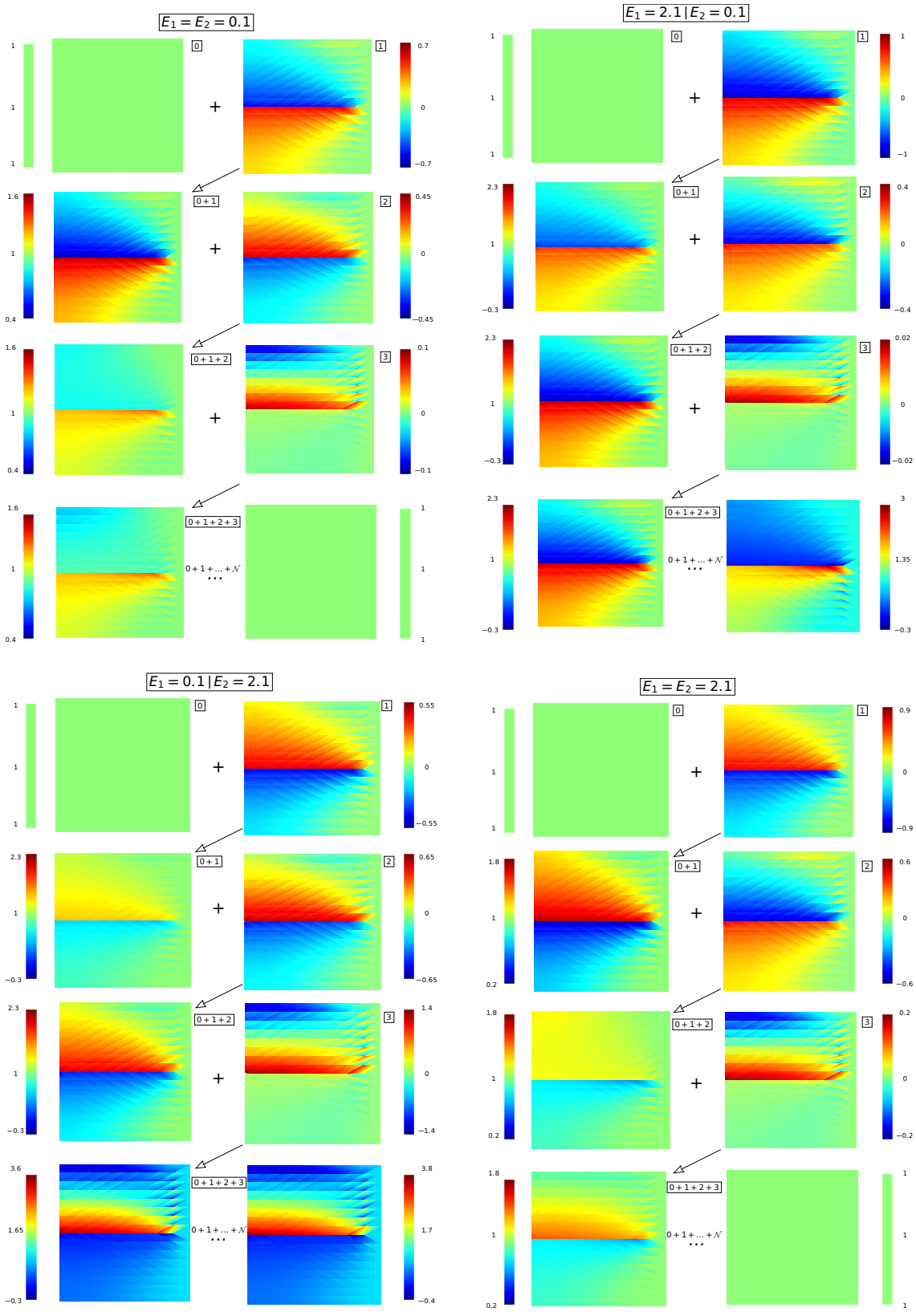


Figure 4: PGD construction of the solution for the equilibrated stress component $\sigma_{xx}$, presenting the solutions with the first 3 PGD modes. Uniform mesh: $n_e = 256$. Approximation functions of degree 1.

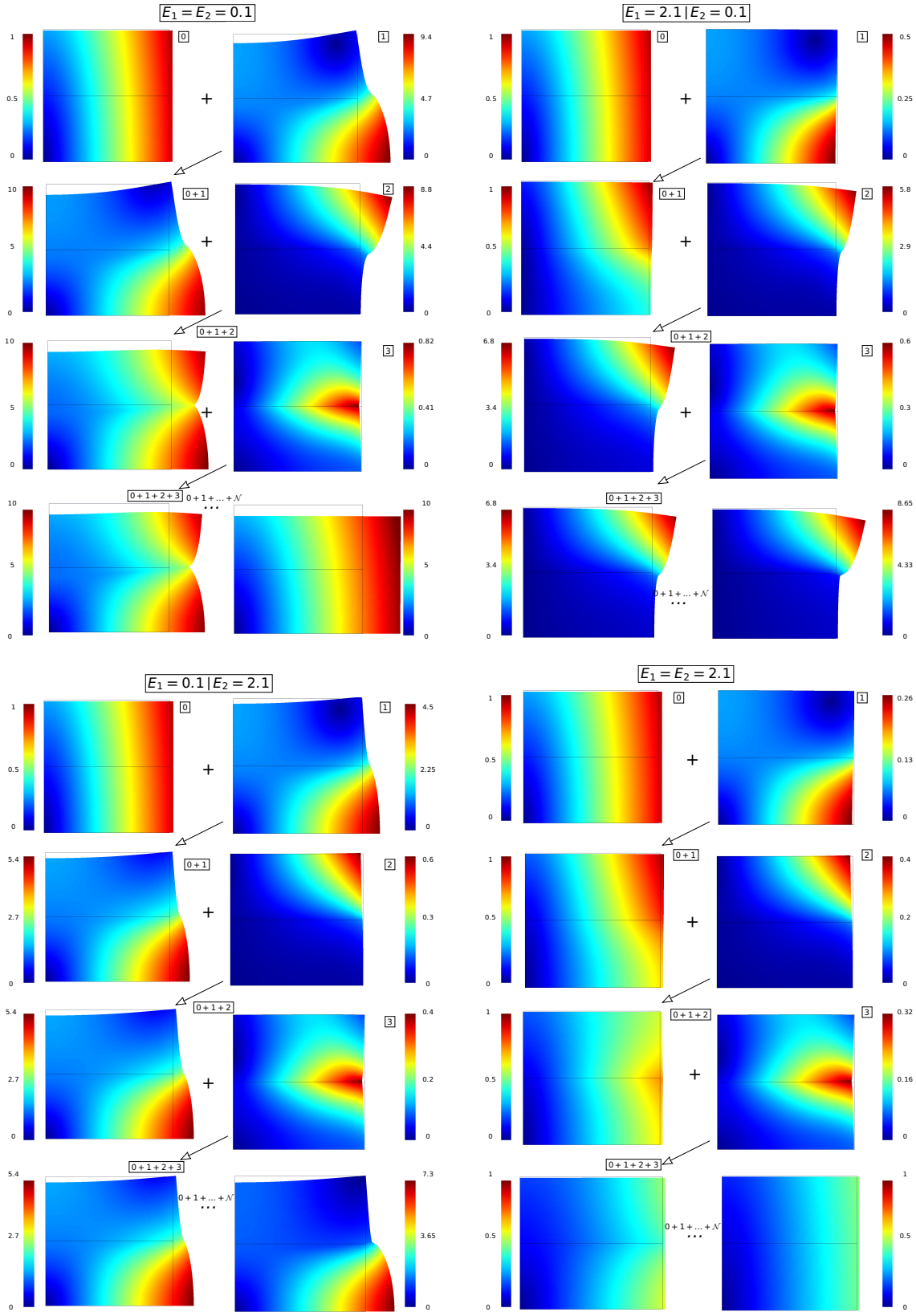


Figure 5: PGD construction of the solution for the compatible displacement field $u$, presenting the solutions with the first 3 modes. Uniform mesh: $n_e = 256$. Approximation functions of degree 2.

Fig. 6 shows the stresses developed at bottom and left supports when the materials have extreme opposite values for the Young's modulus.

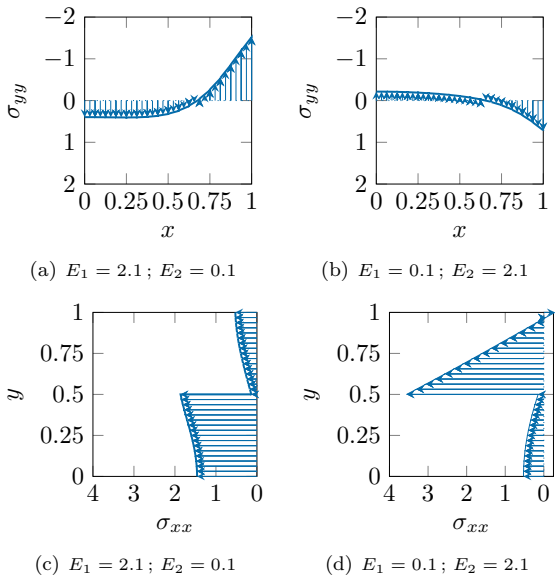


(a) $E_1 = 2.1\,;\, E_2 = 0.1$ (b) $E_1 = 0.1\,;\, E_2 = 2.1$

(c) $E_1 = 2.1\,;\, E_2 = 0.1$ (d) $E_1 = 0.1\,;\, E_2 = 2.1$

Figure 6: $1^{st}$ row: Stress $\sigma_{yy}$ distribution developed at the bottom side support; $2^{nd}$ row: Stress $\sigma_{xx}$ distribution developed at the left side support. Uniform mesh: $n_e = 1024$.

The resultants of both stress distribution at the bottom support respect $\int_0^1 \sigma_{yy}\, dx = 0$, since there isn't any vertical load applied to the plate. While for the stress distribution at the left support, its resultant balances the unit traction, as $\int_0^1 \sigma_{xx}\, dy = 1$.

### 4.2. Quantities of Interest ($QoI$)

We start by looking at the value of the moment reaction at the left support of the plate $\mathcal{M}_1$. Fig. 7 illustrates the virtual problem used for obtaining that $QoI$, which corresponds to imposing at the plate's left side a unit rotation.

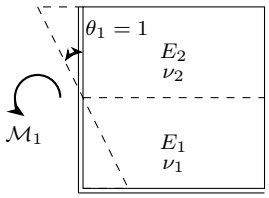


Figure 7: Virtual problem scheme for obtaining the moment reaction at the left support.

Fig. 8 presents the value of $\mathcal{M}_1$ and its bounds, for various combinations of the Young's modulus, which are detailed in Fig. 9.

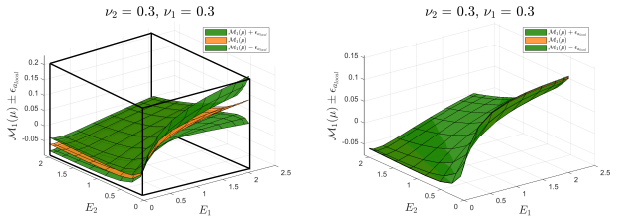


(a) uniform: $n_e = 16$ (b) uniform: $n_e = 1024$

Figure 8: Values of the moment reaction $\mathcal{M}_1$ and its bounds.

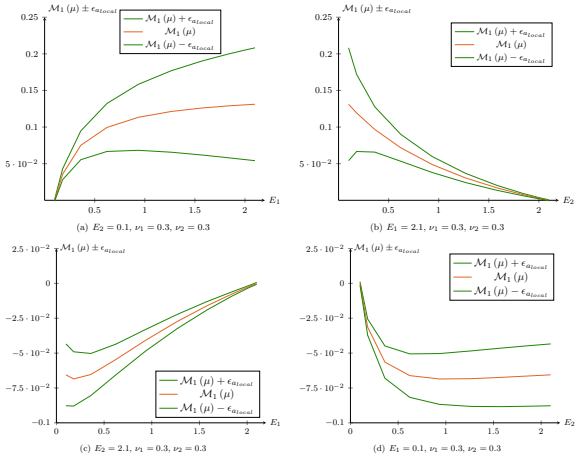

Figure 9: Cut sections for the graph presented in Fig. 8(a), at $E_2 = 0.1$, $E_1 = 2.1$, $E_2 = 2.1$ and $E_1 = 0.1$

It can be seen in Fig. 8 and Fig. 9, that the absolute value of the moment reaction is greater when the bottom part is stiff and the upper flexible. The values are zero when both materials have equal Young's modulis. Using a mesh with more elements, as shown in Fig. 8(b), the bounds become smaller.

Driving an adaptive refinement process based on the global and local error indicators, using the reaction moment as the $QoI$, the meshes in Fig. 10 are obtained:

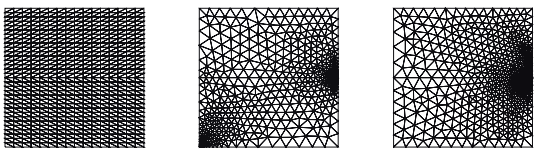

(a) *uniform* : $n_e = 1024$ (b) *local* : $n_e = 1070$ (c) *global* : $n_e = 1379$

Figure 10: Finite element meshes obtained by uniform refinement and by driving an adaptive refinement process based on the global and local error indicators, using the moment reaction at the left side as the $QoI$.

It is observed that the mesh obtained based on the global error indicator captures the transition of mechanical properties, while the mesh obtained based on the local error indicator, also captures the effect of the virtual problem, with more elements at bottom left corner.

Fig. 11 shows the bounds of the error in the moment $\mathcal{M}_1$ for all the combinations of the parameter values. The mesh obtained by uniform refinement has the largest error bounds compared with the others two, while using the mesh obtained based on the local error indicator has the smallest error bounds, as expected.

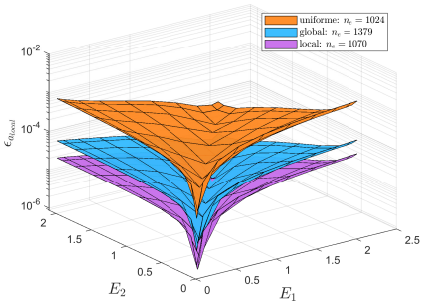


Figure 11: Error Bounds of the moment $\mathcal{M}_1$ for all the combinations of the parameters values. The values are presented for the meshes shown in Fig. 10.

The displacement at the top side of the plate is another *QoI* to consider. Fig. 12 illustrates the virtual problem used to obtain that output. For a homogeneous problem, this value has the exact solution presented in Tab. 1.

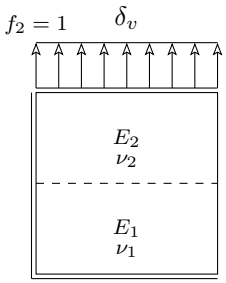


Figure 12: Virtual problem scheme for obtaining the average displacement output at the top side

| $E$ | $\nu$ | $\delta_v$ exact |
|---|---|---|
| 2.1 | 0.3 | 0.14286 |
| 0.1 | 0.3 | 3 |

Table 1: Exact solution of the homogeneous problem, presented for fixed $\nu$ and extreme $E$ values.

Fig. 13 presents the value of $\delta_v$ and its bounds, for all the combinations of the parameters values.

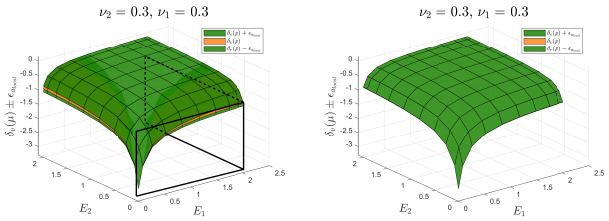


(a) uniform: $n_e = 16$ (b) uniform: $n_e = 1024$

Figure 13: Values of the vertical displacement at the top side $\delta_v$ and its error bounds.

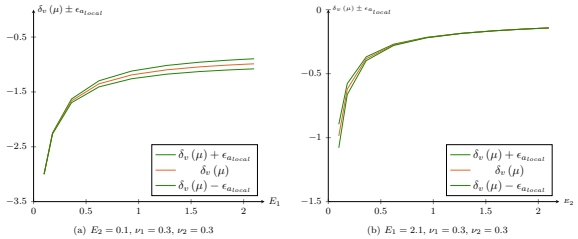


(a) $E_2 = 0.1, \nu_1 = 0.3, \nu_2 = 0.3$ (b) $E_1 = 2.1, \nu_1 = 0.3, \nu_2 = 0.3$

Figure 14: Cut sections for the plot presented in Fig. 13(a), at $E_2 = 0.1$ and $E_1 = 2.1$

As seen in Fig. 13, we have higher value for the displacement at the top side when the two materials are flexible and the smaller value when the two materials are stiff. For all the other cases the displacements are between those two. As can be seen better in Fig. 14, higher values for the error bounds occur when the two materials have extreme opposite values of the Young's modulus and smaller when they are equal.

Tab. 2 summarizes the integrals of the error bounds, involving the two *QoI's* previously considered. The values of the integrals presented for each *QoI*, are obtained using the meshes presented in Fig. 10. $\Psi_{global}$ is smaller for the mesh based on the global error indicator. The mesh based on the local output error provides smaller value of the integral $\Psi_{local}$ for the output $\mathcal{M}_1$, from which it was obtained.

| uniform $n_e = 1024$ | global $n_e = 1070$ | local $n_e = 1379$ |
|---|---|---|
| $\Psi_{global}$ | $\Psi_{global}$ | $\Psi_{global}$ |
| $1.90 \times 10^{-3}$ | $3.02 \times 10^{-5}$ | $6.53 \times 10^{-5}$ |

| | uniform $n_e = 1024$ | global $n_e = 1070$ | local $n_e = 1379$ |
|---|---|---|---|
| *QoI* | $\Psi_{local}$ | $\Psi_{local}$ | $\Psi_{local}$ |
| $\mathcal{M}_1$ | $1.72 \times 10^{-7}$ | $2.18 \times 10^{-9}$ | $3.60 \times 10^{-10}$ |
| $\delta_v$ | $4.27 \times 10^{-7}$ | $8.79 \times 10^{-11}$ | $4.41 \times 10^{-10}$ |

Table 2: Integrals of the error bounds for $\mathcal{M}_1$ and $\delta_v$, using the meshes in Fig. 10.

## 5. Plate fixed at both ends

Fig. 15 shows the second practical problem analised, with the model of the plate (left) as a function of the geometry parameters $a$ and $b$ and its symmetry simplification (right). Fig. 15 also shows the *QoI* to be considered $\delta_V$, that corresponds to the weighted average of the vertical displacement at the plate's middle span.

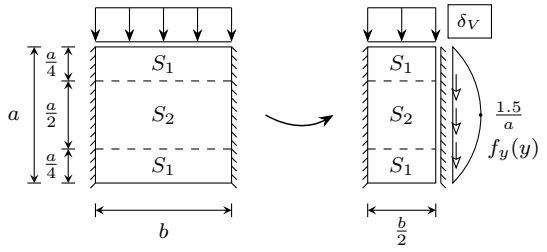


Figure 15: Plate fixed at both ends (left) and symmetry simplification (right). Virtual problem for obtaining the average vertical displacement $\delta_V$ at the plate's middle span.

Using the geometry parameters relation ($a = b = 1$), typical meshes are shown in Fig. 17 and the integrals of the error bounds during the adaptive process are presented in Fig. 16.

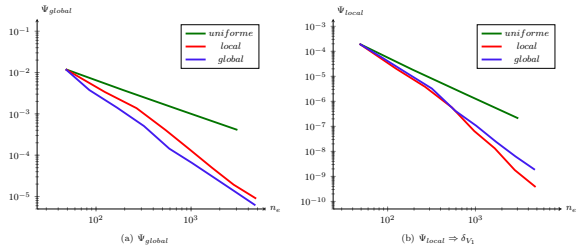


Figure 16: Integrals of the error bounds, as a function of the number of elements for the meshes obtained by uniform refinement and the refinements based on the global and local output error indicators. ($a = b = 1$).

As seen in Fig. 16, the meshes obtained by uniform refinement have the higher values of both integrals, and so, higher error bounds for the global and local output solutions. It can also be seen in Fig. 16, that the meshes based on the global error indicator leads to smaller global error bounds, while using the meshes obtained based on the local error indicator leads to smaller results for the local output error bounds.

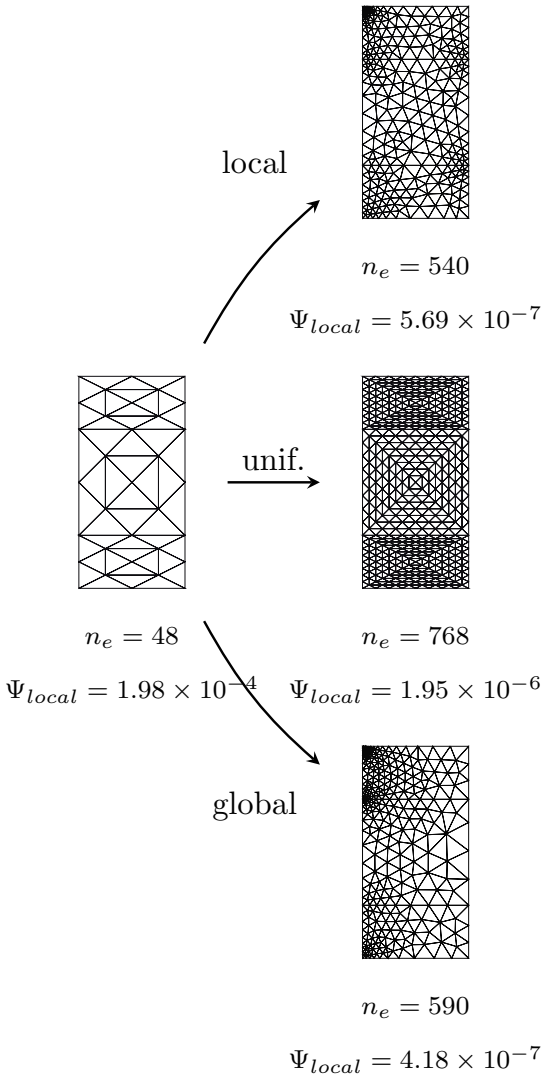


Figure 17: Schematic representation of the meshes obtained by an uniform refinement and the refinements driven by the global and local output error indicators. ($a = b = 1$).

From Fig. 17, is seen that the meshes based on the global error indicator are able to capture the, transition of mechanical properties and geometric singularities, while the meshes obtained based on the local output error indicator, also captures the effect of the virtual load in the solution.

Fig. 18 shows the displacement at the plate's middle span for all combinations of the parameters values and its bounds, which are detailed in Fig. 19. It can be seen again that the higher value of displacement occurs when the materials are flexible and smaller when they are stiff. From the same

set of figures, it can be seen that the highest error bounds occur when the materials have extreme opposite values of the Young's modulus and smaller for the cases where they are equal.

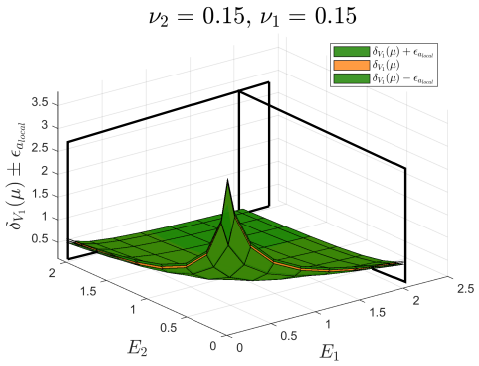


Figure 18: Values of the displacement $\delta_{V_1}$ and its bounds for all combinations of the parameters values. $(a = b = 1)$ ; Uniform mesh: $n_e = 48$.

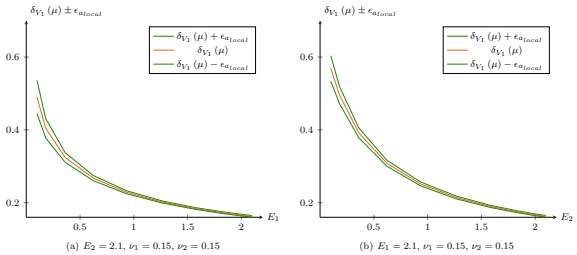


Figure 19: Cut sections for the plot presented in Fig. 18, at $E_2 = 2.1$, $E_1 = 2.1$.

Fig. 20 shows the stress diagrams at the plate's middle span when Young's modulus values are extreme opposite and when they are equal. The cases presented in Figs. 20(a) and 20(b), exhibit stress descontinuities at material transitions and high stress values at stiff materials' top and bottom fibre. While the cases where the Young's modulus are equal, the stress diagram exhibits a smooth distribution along the height without descontinuities and with the maximum values at the top and bottom fibres as predicted by the elementary beam theory for a homogeneous cross section.

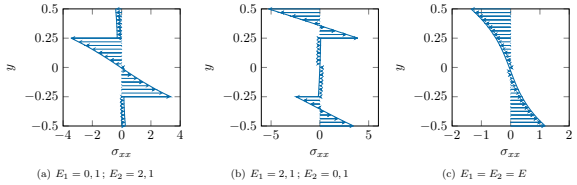


Figure 20: Stress diagrams $\sigma_{xx}$ at the plate's middle span for specific combination of the parameters values. $(a = 1; b = 2)$. Uniform mesh: $n_e = 512$.

## 6. Conclusions and Future Studies

One of the essential characteristics of the PGD worth remarking, which allows it to deal with high-dimensional models without major issues, is the separated representation of the solution of the problem and the advantage that this represents, particularly in the evaluation of integrals.

In general, for the problems analysed, it was seen that the number of modes required to yield an accurate solution turns out to be smaller than a few dozens. This also holds when using finer meshes, however, for a given level of accuracy, they generally imply more modes until convergence is reached. It is also observed that higher values for the bounds of the error of the local outputs occur in general when the materials have extreme opposite values of the Young's modulus and these are smaller when they are equal. Finally, using a mesh adaptivity process oriented for a given quantity of interest, led in general to smaller values for the error on that local output than an uniform refinement or the refinement based on either the global error indicator or the local error indicator for another quantity. Using the global error indicator to drive the adaptivity process led to smaller global errors for the solutions and to a balance between the different local error bounds. In the particular context of structural mechanics, one subject proposed for further development is obtaining solutions for simple problems as a function of the geometry parameters. However, obtaining a separated representation for those can be a complicated task.

## References


[1] L. Chamoin, P. Ladeveze, and F. Pled. Recent advances in the control of PGD-based approximations. $6^{th}$ *International Conference on Adaptive Modeling and Simulation*, pages 170–181, June 2013. doi:hal-01057247.

[2] F. Chinesta, A. Ammar, and E. Cueto. Recent advances and new challenges in the use of the proper generalized decomposition for solving multidimensional models. *Archives of Computational Methods in Engineering*, 17:327–350, 12 2010.

[3] J. Reis. *Error Estimation and Adaptivity for PGD Solutions*. Tese de Doutoramento, Universidade de Lisboa, Lisboa, 2020.

[4] J. Reis, J. P. Moitinho de Almeida, P. Díez, and S. Zlotnik. Error estimation for proper generalized decomposition solutions: Dual analysis and adaptivity for quantities of interest. *International Journal for Numerical Methods in Engineering*, 122(3):752–776, 2021.